sciendo

LATVIAN JOURNAL OF PHYSICS
AND TECHNICAL SCIENCES
2023, N 4

DOI: 10.2478/lpts-2023-0021

ADAPTIVE FAULT LOCATOR FOR HIGH-VOLTAGE TRANSMISSION LINES BASED ON THE ESTIMATION OF POWER SYSTEM MODEL PARAMETERS

I. Zalitis, A. Dolgicers, J. Kozadajevs, J. Berkolds

Riga Technical University, Institute of Power Engineering
12-k1 Azenes Str., Riga, LV-1010, LATVIA
*e-mail: ivars.zalitis@rtu.lv

This paper presents an adaptive transmission line fault location method, which incorporates fault location devices at both line ends and utilises data import from a supervisory control and data acquisition system without strictly requiring data synchronisation. The developed method aims at achieving a higher degree of robustness, adaptiveness and accuracy. The adaptiveness is achieved by dynamic updating of mathematical models used on the basis of network-wide information, such as data on the state of circuit-breakers and apparent power at load and generation nodes. The robustness and accuracy are enhanced by incorporating two stages of identification of model parameters with the goal of reducing the decision variable space for the stage identifying fault parameters. Furthermore, in addition to utilisation of all measurements available at a particular substation, the developed method partially employs the measurements from the other end of the line by means of result cross-checks, but does not require a full data set, unlike deterministic-model-based methods. An optimisation-based approach, redundancy on the basis of extended measurement set, and cross-checks reduce the risk of fault location errors due to measurement errors or "voids" in the data available. Testing of the developed method demonstrates its accuracy and robustness in a wide range of pre-fault and fault regime scenarios, even when considering various pre-fault contingencies.

Keywords*: Fault location*, *modelling*, *optimisation, transmission lines*.

1. INTRODUCTION

Research has led to the development of various fault location (FL) techniques for high-voltage (HV) overhead transmission lines (OHTLs). First, one-terminal-measurement-based (OTMB) methods with fault loop impedance measurements were developed [1]. The improved digital device adaptation of this approach [2] is still in use in parts of the Baltic power systems. In contrast to the developed one, these methods are simpler and easier to implement, but they sometimes prove inaccurate due to the reactance effect [3], [4]. Additionally, if mismatching results of such FL devices from both substations are used, it requires experienced personnel to determine the correct fault location, which is avoided by the developed method.

Introduction of communication networks between different substations made measurements from both terminals available for use with corresponding fault point voltage equations to directly calculate the fault distance at once. One of these two-terminal-measurement-based (TTMB) methods utilises negative-sequence (NS) current and voltage phasors obtained at both line terminals [2], a different one uses both the positive-sequence (PS) and NS phasors [5]. TTMB methods are easy to implement and in most cases, they are more accurate than OTMB methods because they negate the reactance effect. The two equations of the voltage at the fault point are sometimes kept separate and optimisation is used to minimise the difference of the results obtained from them [6]–[8]. Both approaches are dependent on precise synchronisation of measurements during the fault and the reliability of the communication network. Falling trees, with a high probability, can damage not only the power line but also the communication cable attached to it, making such FL designs less reliable compared to the presented method. A method similar to [6]–[8], which also estimates the shift angle of unsynchronised measurements, has been proposed in [9]. This method can potentially avoid the problem of measurement synchronisation, but there is a risk that the estimated angle will be shifted by one or more periods, which could introduce errors if the fault path resistance is not stationary (e.g., faults caused by fallen trees, especially pines and similar trees).

Wide interest has also been devoted to the travelling-wave (TW) FL methods. Most TW methods determine the fault distance by either measuring the time required for the transient fault wave with a known wave propagation velocity to reflect from the fault location [10], [11] or the difference between the wave arrival times at both substations. TW methods are considered accurate but they require good correlators to recognise the actual fault wave and avoid errors caused by wave distortions due to irregularities of the power system or wave decay [12], [13]. Methods that apply an optimisation with measurements of fault transients have been proposed for FL as well [7], [14]; however, these methods, as well as the original-type TW methods, require a high sampling frequency resulting in more expensive devices, which is not required for the developed method.

A different group of methods is based on artificial neural networks (ANNs) [15]–[17]. ANNs provide an opportunity for performing different functions simultaneously, such as identification of the fault type and fault location, with a satisfactory accuracy.

These methods are promising [18] but they require an extensive training database and can be complicated to implement. A similar OTMB method using the k-nearest neighbour technique [19], which only uses voltage signal measurements, obtains the harmonic spectrum of this signal, and then uses a database of similarly processed recordings to recognise the fault location. This allows avoiding problems associated with communication networks and potential current transformer saturation; however, this method requires a high sampling frequency and a sufficient database of fault recordings. In comparison to these methods, the developed method only requires basic network data and periodic updates on the network structure and the power generated and consumed at the modelled nodes.

A FL method based on Monte-Carlo optimisation is also known [20]. This OTMB method replaces the unknown impedance of the remote-end power system with a probability distribution of its values and filters out solution variants that imply reactive power consumption at the fault location. This approach can be easily adapted to different fault types and retains a satisfactory accuracy even in cases when line-specific parameters vary, but it has a very high computation cost and papers that present this method do not consider complex line configurations.

This paper presents a future study on the parameter-estimation-based FL method [13]. The goal of this research is to make the previously developed method more adaptive, robust and accurate, first, by introducing automatic updates of the models, corresponding measurement data sets, and model outputs used, and by additional estimation of sequence impedances of the equivalent power system when network simplifications are employed. These improvements provide an ability to reflect changes of network topology due to disconnections of network elements prior to a fault not only in the exactly modelled part of the network, but also in network parts represented by an equivalent power system. Dynamic model updates are made on the basis of data from a supervisory control and data acquisition (SCADA) system. This includes the state of circuit breakers (CBs) to make the model graph match the actual system in exactly the modelled part, and apparent power at the connection nodes of modelled equivalent generation and load is also fetched from SCADA. Apparent powers are used directly in the model utilised by the first parameter estimation stage and later to determine generator electromotive forces (EMFs) and to calculate equivalent impedances representing loads for the model used by the second estimation stage. Furthermore, one extended model considering faults at any transmission line in a precisely modelled network part can now be used for several substations. None of the data requested from a SCADA system have strict requirements regarding synchronisation or transfer speed. Secondly, a further improvement is achieved by performing cross-checks of results obtained by individual FL devices at both ends of the faulted line before the selection of the best solution variant. The case study, which considers not only changes in network topology prior to a fault but also different pre-fault and fault scenario combinations, demonstrates the capabilities of the developed method.

Section 2 presents the new adaptive features and the methodology applied. Section 3 describes the case study network and discusses the obtained results. Finally, conclusions are provided.

2. AN ADAPTIVE FAULT LOCATION BASED ON TWO STAGES OF SYSTEM MODEL PARAMETER ESTIMATION

2.1. New Adaptive Features of the Developed Method

In order to overcome limitations imposed by the incomplete scope of information available to an OTMB FL device, and to make the developed FL method more adaptive while avoiding a requirement for exchanging precisely synchronised data, several options are chosen.

First, an ability to adapt models used for the two estimation stages prior to a fault is integrated in the developed method utilising indications of states of CBs from a SCADA system and element IDs assigned to each branch and at least part of the nodes of the equivalent circuits used. When disconnections of network elements split a model of a pre-fault state, the network parts that do not include FL devices controlling a faulted line are removed from the updated versions utilised for both pre-fault and fault state models to save computation time. While the accuracy of many existing FL methods is unaffected (e.g., TTMB methods [6]–[9],) or can even potentially improve (e.g., simple OTMB methods [1], [2]) in case of such pre-fault contingencies, the accuracy of methods such as those using ANNs, if the training database used does not include faults after contingencies, or those estimating the impedance of the equivalent power system as connected at the end of the line [20], if the other end of the line were to be disconnected, may be degraded.

Second, the developed method also requires the apparent powers of generators and loads available for corresponding nodes in both of the models used. These can be estimated [13], if necessary, but that increases the computation cost and the risk of errors, so measured data will be welcomed. In the pre-fault state model used by the first estimation stage, all of these apparent powers are included as power demand or injections at their respective nodes based on element IDs and node types (demand, power losses, constant power generation, generation with the possibility of power balancing). The only exception is when a pre-fault contingency breaks a link between a network part including relevant FL devices and an equivalent power system. In this case, if there is at least one source capable of balancing power in the remaining network part, one of the said sources is modelled as a constant EMF (balancing) source while others will remain as power injections. In order to achieve this, the model of the pre-fault state was changed from the one used previously [13] to one that operates with phase-to-earth voltages and employs earth as the base node of an equivalent circuit. The apparent powers of demand and generator nodes are also used for the model of the fault state, where equivalent load impedances are updated and generator powers are used to estimate generator EMFs at the moment of fault occurrence. The described model updates using SCADA data take place periodically before the occurrence of a fault, making both models updated near real time but without a strict synchronisation requirement for data exchange.

2.2. Estimation of Unknown Model Parameters

Both estimation stages are defined as optimisation tasks, which minimises the difference between the measurements from the controlled substation and the corresponding outputs of a mathematical model of the power system. The overall goal for both estimation stages is to determine their respective unknown model parameters with the best possible accuracy and within reasonable computation time. However, a strict limit of a maximum error of 5 % is only applied to the fault distance estimate, as estimation of other parameters is of secondary importance.

The first estimation stage is active before a fault occurs. and its purpose is to reduce the number of unknown parameters for the second estimation stage by determining the PS impedance of an equivalent power system, if such a simplification is used. As the NS current circulation paths coincide with PS ones, an estimate of a PS impedance also allows greatly limiting the expected values of an NS impedance. This is possible because the main reason for their difference is the dissimilarity between PS and NS impedances of rotating electric machines, which are well defined [21]. This stage uses phasors of the calculation phase obtained from processed measurement recordings of substation bus voltages and currents as well as power flows from all the branches connected to the substation buses.

These values are automatically compared to the corresponding outputs of a mathematical model of a pre-fault state. Next, a "difference" value, Δ, is calculated, which is utilised here as a conceptual representation of the actual objective function f_{OBJ} (Subsection 2.3). When the convergence criteria are met for the optimisation at both ends of the faulted line, the obtained solution variants are exchanged between FL devices for a cross-check (Subsection 2.3) before the selection of a final estimate. The PS impedance obtained is then used to update the pre-fault state model utilised to estimate generator EMFs. Next, the estimated PS impedance of an equivalent power system and generator EMFs are updated in the fault state model. At the same time, the PS impedance is used to set limits to potential values of the modulus and the X/R ratio of the NS impedance of the power system for the second estimation stage:

$$\begin{cases} 0.18\left|\dot{Z}^1_{\mathrm{SYS}}\right| \le \left|\dot{Z}^2_{\mathrm{SYS}}\right| \le 0.42\left|\dot{Z}^1_{\mathrm{SYS}}\right| \\ 0.1\,X^1_{\mathrm{SYS}}/R^1_{\mathrm{SYS}} - 2 \le X^2_{\mathrm{SYS}}/R^2_{\mathrm{SYS}} \le 0.4\,X^1_{\mathrm{SYS}}/R^1_{\mathrm{SYS}} + 2 \end{cases}, \tag{1}$$

where $\dot{Z}^1_{\mathrm{SYS}}$ – the estimated PS impedance of an equivalent power system, Ω; $\dot{Z}^2_{\mathrm{SYS}}$ – the NS impedance of an equivalent power system, Ω; R^1_{SYS}, R^2_{SYS}, X^1_{SYS}, X^2_{SYS} – the active and reactive components of $\dot{Z}^1_{\mathrm{SYS}}$ and $\dot{Z}^2_{\mathrm{SYS}}$, respectively, Ω.

The limits (1) are introduced by considering several factors. Firstly, on average for different generators, moduli of $\dot{Z}^2_{\mathrm{G}}$ constitute approximately 10 %–20 % of moduli $\dot{Z}^1_{\mathrm{G}}$ and ratios $X^2_{\mathrm{G}}/R^2_{\mathrm{G}}$ constitute 2 %–13 % of $X^1_{\mathrm{G}}/R^1_{\mathrm{G}}$ at steady-state conditions [21]. Secondly, the difference between PS and NS impedances is assumed lower than that for generators, considering that there should be a substantial number of connecting elements between remote generators and the busbars of an equivalent power system for one to

employ such a simplification. Thirdly, the limits are then slightly extended by 2 % and 2 p.u. to account for potential errors of the estimated $\left|\dot{Z}^1_{\mathrm{SYS}}\right|$ and $X^1_{\mathrm{SYS}}/R^1_{\mathrm{SYS}}$ values.

As can be seen, the first estimation stage both removes one decision variable for the estimation of fault state parameters and limits the search space for a second one, thus improving the robustness and accuracy of the developed method. Addition of this stage does increase the total computation cost; however, this is partially offset by the reduced search space for the second stage and it does not increase the FL time as the first stage is active only before a fault occurs.

The second estimation stage is activated when a fault is cleared and measurement signals have been processed by removing the free decaying component (DC offset) and extracting phasors of the fundamental frequency [22] from the first full cycle. This part of signal recordings is chosen to minimise the possible differences between the values of EMFs used in a fault state model and actual EMFs due to potential electromechanical transients. The second estimation stage is tasked with estimation of fault distance α, equivalent fault path resistance R_{F}, NS, and zero-sequence (ZS) impedance of an equivalent power system $\dot{Z}^0_{\mathrm{SYS}}$. For calculating the objective function, the following phasors and values are determined and used separately by FL devices at both ends of a faulted OHTL:

- The phase voltages of busbars at the substation where the FL device is installed, and symmetrical components of the calculation phase derived from them;
- Phase currents for each branch connected to the substation and symmetrical components of the calculation phase currents derived from them;
- The symmetrical components of the calculation phase apparent power for each branch connected to the substation;
- The fault distance that would be analytically calculated by an existing OTMB FL method.

All of the phasors obtained from each of the branches that are connected to the substation are automatically arranged in a vector using an updated “relay” terminal (FL device) and element IDs. Thus, both the set of the measurement phasors and the results of the steady-state simulations automatically retain correct order and match an up-to-date pre-fault network topology. The fault distance estimate included as one of the measurements uses apparent reactance for a distance calculation and is implemented in an existing relay terminal [2]. For phase-to-earth faults in parallel OHTL, this distance is calculated according to the following equation:

$$\alpha = \mathrm{Im}\left(\dot{U}_{\mathrm{Fph}}/\dot{I}^0_{\mathrm{FL}}\right)/\left(\mathrm{Im}\left(\dot{Z}^1_{\mathrm{L1km}}\left[\dot{I}_{\mathrm{Fph}} + \dot{k}_{0\mathrm{FL}}\dot{I}^0_{\mathrm{FL}} + \dot{k}_{0\mathrm{M}}\dot{I}^0_{\mathrm{PL}}\right]/\dot{I}^0_{\mathrm{FL}}\right)L_{\mathrm{L}}\right), \quad (2)$$

where α – the fault distance, p.u.; $\dot{U}_{\mathrm{Fph}}$ and $\dot{I}_{\mathrm{Fph}}$ – the faulted phase voltage and current of the faulted line, V and A; $\dot{I}^0_{\mathrm{FL}}$ and $\dot{I}^0_{\mathrm{PL}}$ – the ZS currents of the faulted line and the healthy parallel line, A; $\dot{Z}^1_{\mathrm{L1km}}$ – the PS impedance of a one-kilometre-long section of the faulted line, Ω; $\dot{k}_{0\mathrm{FL}}$ – a ZS compensation coefficient, p.u.; $\dot{k}_{0\mathrm{M}}$ – the ZS mutual induction compensation coefficient (the ratio between the impedance of ZS mutual induction between both lines and the PS impedance of the faulted line), p.u.

When other fault types are considered, a similar OTMB FL formula would be used instead.

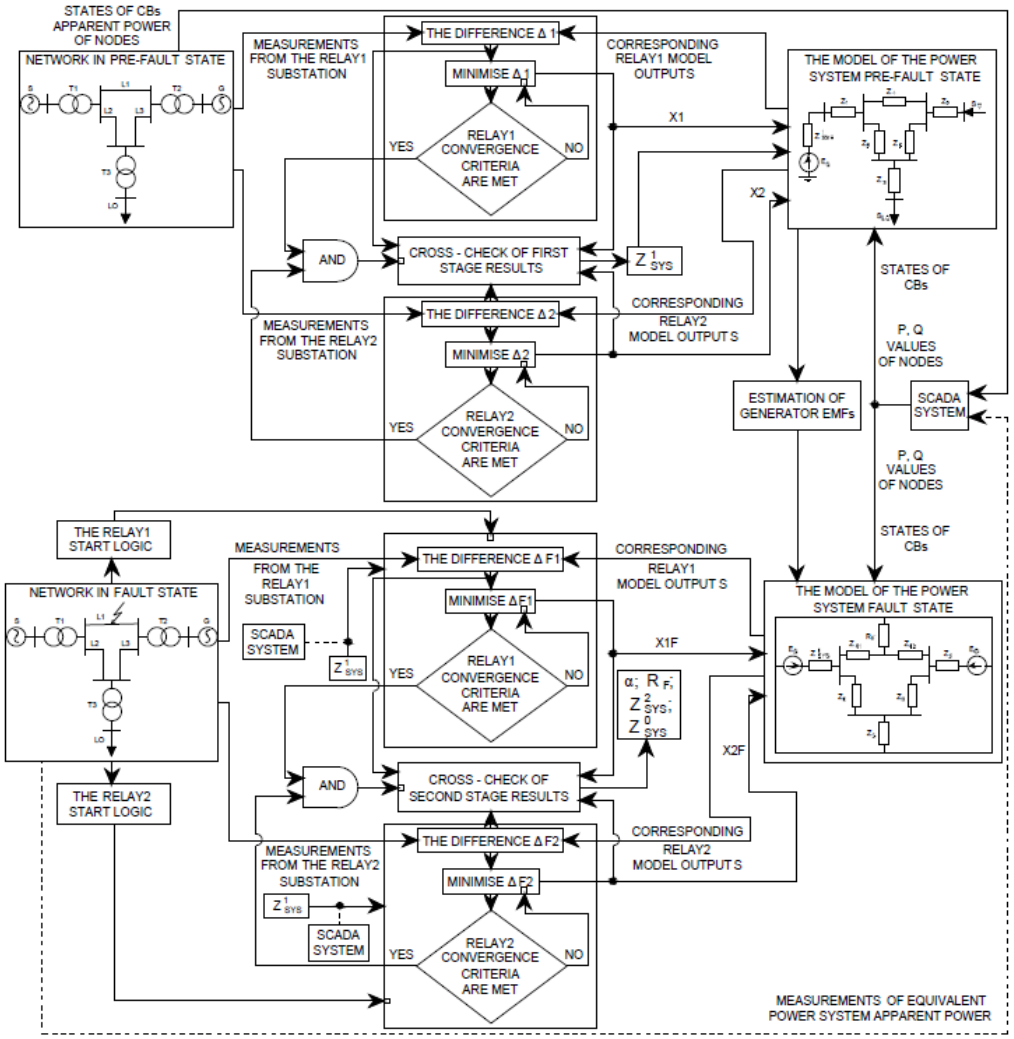

Fig. 1. The flowchart of the developed method.

When the convergence criteria of the optimisation for the second stage are met, a more rigorous cross-check is performed using the solution variants generated by FL devices at both ends of the line before selecting the most fitting solution overall. Finally, the value of α is extracted from the obtained group of decision variable values. The described framework using two stages of model parameter estimation with their respective solution cross-checks is presented as a flowchart below (Fig. 1). In the figure, X1, X2 represent decision variable vectors for the first and second "relay" terminal, respectively, which together provide a PS impedance of an equivalent power system, Z^1_{SYS}. X1F, X2F are decision variable vectors for the second (fault state) estimation stage. As can be seen in Fig. 1, an alternative version of the developed method

is also considered in this study. It utilises additional measurements of apparent power flowing from an equivalent power system to its busbars for both estimation stages. The alternative version is analysed as a potential solution for rare cases where errors of estimated power system equivalent impedance might impact the overall FL accuracy and in order to see how much the additional measurement data affect the parameter estimation accuracy. However, it is still expected of the developed method to provide fault distance estimates with the aforementioned 5 % tolerance limit in all conceivable operational scenarios even without apparent power measurements added. Regardless of utilisation of the additional measurement data used for the model, updates and cross-checks do not require high-speed or synchronised communication channels between relay terminals at both ends of the faulted line. As a result, the FL in these terminals operate practically independently, except for cross-checking the obtained results.

Employing an optimisation, using measurements available from all the branches connected to a particular substation and integrating limited communication between FL devices and the SCADA system, the developed method can provide accurate fault distance estimates while avoiding dependence on the exchange of high-speed, synchronised measurement data.

2.3. The Optimisation Techniques and Cross-Checks Employed

An optimisation is utilised to determine the unknown parameters of a mathematical model by minimising the difference, Δ, between phasors obtained from measurement data and those calculated by using updated models of the considered network part. The actual objective function is calculated as the sum of squared relative errors of the real and imaginary part of each phasor separately. Thus, the optimisation task is defined as

$$\min_{f_{\mathrm{OBJ}}\in[0,\infty)} \sum_{i=1}^{N_{\mathrm{MEA}}} \left[K_{\mathrm{W}i} \cdot \left(\left(\frac{\mathrm{Re}(y_i)-\mathrm{Re}(y_{\mathrm{m}i})}{|y_i|}\right)^2 + \left(\frac{(\mathrm{Im}(y_i)-\mathrm{Im}(y_{\mathrm{m}i}))}{|y_i|}\right)^2\right)\right], \tag{3}$$

where $K_{\mathrm{W}i}$ – the weight coefficient of the i-th measured parameter; N_{MEA} – the number of measurements used for the estimation process; y_i – the phasor value of the i-th measured parameter; $y_{\mathrm{m}i}$ – the phasor of the corresponding model output of the i-th parameter.

If the modulus of a phasor obtained from measurements is $|y_i| = 0$, the relative difference is determined by using $|y_{mi}|$ as a base in (3). Optimisation as shown in (3) is applied for both estimation stages with decision variables being $|Z^1_{\mathrm{SYS}}|$; $X^1_{\mathrm{SYS}}/R^1_{\mathrm{SYS}}$ for the first stage and α; R_{F}; $|\dot{Z}^2_{\mathrm{SYS}}|$; $X^2_{\mathrm{SYS}}/R^2_{\mathrm{SYS}}$; $|\dot{Z}^0_{\mathrm{SYS}}|$; $X^0_{\mathrm{SYS}}/R^0_{\mathrm{SYS}}$ for the second stage, respectively. During the first estimation stage, the optimisation has to adhere to the following limits:

$$0.5|\dot{Z}^1_{\mathrm{SYS\,N}}| \le |\dot{Z}^1_{\mathrm{SYS}}| \le 2|\dot{Z}^1_{\mathrm{SYS\,N}}|, \tag{4}$$

$$6 \le X^1_{\mathrm{SYS}}/R^1_{\mathrm{SYS}} \le 40 \text{ p.u.}, \tag{5}$$

$$0.8U_{\mathrm{N}j} \le |\dot{U}_j| \le 1.5U_{\mathrm{N}j}, j = 1, \ldots, N_{\mathrm{NODES}}, \tag{6}$$

and during the second stage, the limits applied are as follows:

$$0.001 \leq \alpha \leq 0.999 \text{ p.u.}, \tag{7}$$

$$0.1 \leq R_{\mathrm{F}} \leq 200\ \Omega, \tag{8}$$

$$0.5\left|\dot{Z}^{2}_{\mathrm{SYS\,N}}\right| \leq \left|\dot{Z}^{2}_{\mathrm{SYS}}\right| \leq 2\left|\dot{Z}^{2}_{\mathrm{SYS\,N}}\right|, \tag{9}$$

$$3 \leq X^{2}_{\mathrm{SYS}}/R^{2}_{\mathrm{SYS}} \leq 30 \text{ p.u.}, \tag{10}$$

$$0.5\left|\dot{Z}^{0}_{\mathrm{SYS\,N}}\right| \leq \left|\dot{Z}^{0}_{\mathrm{SYS}}\right| \leq 2\left|\dot{Z}^{0}_{\mathrm{SYS\,N}}\right|, \tag{11}$$

$$3 \leq X^{0}_{\mathrm{SYS}}/R^{0}_{\mathrm{SYS}} \leq 30 \text{ p.u.}, \tag{12}$$

where $\dot{Z}^{1}_{\mathrm{SYS\,N}}$, $\dot{Z}^{2}_{\mathrm{SYS\,N}}$ and $\dot{Z}^{0}_{\mathrm{SYS\,N}}$ – the PS, NS and ZS impedances of an equivalent power system at nominal operation conditions, Ω; $\dot{U}_j$ – the steady-state voltage calculated at node j of the pre-fault model, kV; $U_{\mathrm{N}j}$ – the nominal voltage at node j of the pre-fault model, kV; N_{NODES} – the number of nodes in the pre-fault model.

Limits (4), (9) and (11) are chosen assuming that the most notable possible changes in these impedance values, besides the loss of a link with an equivalent power system, will be due to connection or disconnection of one of two parallel elements. The loose limit (6) is adopted so that testing of the developed method may include even hardly possible post-contingency operation conditions.

Minimisation (3) is achieved with the help of a version of the genetic algorithm (GA). The GA is a versatile optimisation tool and it has been shown to be useful in similar technical tasks with several different types of GA operators and GA algorithm structures known [7], [23]–[25]. This study uses a modified version of the GA applied in [13]; therefore, only the differences introduced with these modifications will be discussed here. The most notable changes to the GA used are to be found in the convergence criteria. In addition to a base requirement of minimum generation count $minN_{\mathrm{GEN}}$ there are now three convergence criteria combinations that lead to the end of the main GA cycle. The first one remains as in [13] and requires the relative difference between the mean and minimum values of fitness or objective function *EPS* and the maximum Hamming distance to fall below certain thresholds *TH1* and *TH2* (20 % and 5 % for the first stage). The second option requires a number of stagnating generations to reach a set limit. The stagnation is recorded when the change in *EPS* between generations is smaller than *TH2* and the change in a minimum value of fitness between generations is smaller than a different stagnation upper limit. Thus, if no progress is achieved, the GA cycle is stopped to save computation time. The third group of criteria requires for the mean and minimum values of the last population fitness to be equal and lower than the minimum fitness value obtained from the initial group of solutions generated randomly before the beginning of the main GA cycle. The first estimation stage testing showed high tolerance, therefore, most of the performance balancing for it is aimed at computation time reduction as indicated by the addition of the second and third convergence criteria groups. Furthermore, the population size and the number of population members chosen via the elite selection approach [13] for this stage have

been reduced to 16 and increased to 75 %, respectively. The step values for the estimation of unknown parameters are set to 0.01 Ω for $|\dot{Z}^1_{\mathrm{SYS}}|$ and 0.1 p.u. for the $X^1_{\mathrm{SYS}}/R^1_{\mathrm{SYS}}$ ratio, respectively.

Due to the accuracy observed, a relatively simple cross-check is applied for this stage to balance any unlikely errors incurred by a FL device at one of the line ends. After exchanging only the single best solution variants and the corresponding values of the objective function, each FL device calculates the value of the objective function for a solution provided by the other device. The relative total objective function (fitness) value is then calculated for each solution:

$$f_{\mathrm{OBJtotal}} = \left(f_{\mathrm{OBJ1}}/f_{\mathrm{OBJbest1}}\right) + \left(f_{\mathrm{OBJ2}}/f_{\mathrm{OBJbest2}}\right), \tag{13}$$

where f_{OBJtotal} – the relative total fitness value of a particular solution variant; f_{OBJ1} and f_{OBJ2} – the fitness values calculated by the first and second FL device using the particular solution variant; f_{OBJbest1} and f_{OBJbest2} – the fitness values for the best solutions in the last population of the GA from the first and the second FL device, respectively.

The solution variant with the lowest f_{OBJtotal} value is chosen or mean values from both solution variants are calculated if both decision variable vectors (solutions) have identical f_{OBJtotal} values.

The second estimation stage utilises the same GA version, but with more stringent settings for convergence criteria. The balancing towards higher accuracy at the expense of an additional computational burden is chosen due to the importance of correct distance estimation and other factors. The stagnating generation is registered if the change in the *EPS* between generations is lower than one-tenth of *TH2*. Additionally, here the third group of criteria is applied if the mean and minimum fitness values are less than one-tenth of the smallest fitness value calculated for the initial randomly generated solution group. The accuracy is further increased by using 20 population members and elite selection of only 50 % of new members. The maximum threshold value of the *EPS* for the first group of convergence criteria is set to 0.5 % and the maximum Hamming distance to 5 %. At the same time, the size of the initially generated group of random solutions is set to 5000 in contrast to 1000 for the first stage.

The step values used for the estimation of unknown fault-state model parameters are 0.001 p.u. and 0.1 p.u. for α and $X^2_{\mathrm{SYS}}/R^2_{\mathrm{SYS}}$, $X^0_{\mathrm{SYS}}/R^0_{\mathrm{SYS}}$ ratios, and 0.01 Ω for R_{F}, $|\dot{Z}^2_{\mathrm{SYS}}|$, $|\dot{Z}^0_{\mathrm{SYS}}|$, respectively. When the GA has converged for both FL devices, they exchange their last populations (solution groups). The maximum and minimum values for each decision variable are determined from all of these solutions. Next, a test group of solution variants is generated by combining pairs of α and R_{F} values with groups of $|\dot{Z}^2_{\mathrm{SYS}}|$, $X^2_{\mathrm{SYS}}/R^2_{\mathrm{SYS}}$, $|\dot{Z}^0_{\mathrm{SYS}}|$, $X^0_{\mathrm{SYS}}/R^0_{\mathrm{SYS}}$ values from the top 10 solutions provided by each FL device. Then, the test group is extended with a large number of randomly generated solutions within the previously determined minimum and maximum values. The resulting test group is then sent to both FL devices, which calculate their objective function values. The final solution is the one with the lowest total relative objective function value calculated according to (13).

As shown by Section 2, the developed method can be described as an optimisation-based recognition of the most likely model parameters utilising measurement data. However, in contrast to other recogni-

tion-based methods [15]–[19], the reference used is an adaptive mathematical model rather than a set of prior measurement data or simulation results. Furthermore, in contrast to OTMB methods, be they analytical [2] or probabilistic [20], the developed method models a wider extent of the neighbouring network and utilises measurements from all the branches connected to the substation. These differences together with the cross-checks introduced in the developed method reduce the risk of FL errors due to errors or insensitivity of measurements at any of the two substations.

3. THE CASE STUDY

3.1. The Case Study Power System

The power system used for studying the operation of the developed FL is presented in Fig. 2. Network sections controlled by relay terminals with the developed FL are shown in blue rectangles. Designations for the modelled OHTL faults are included as well. Detailed information about the network elements is provided in [13]. Four base scenario groups will be analysed with and without utilisation of the additional measurements of apparent power from the equivalent power system S and one scenario group, where the power system is disconnected from the analysed network.

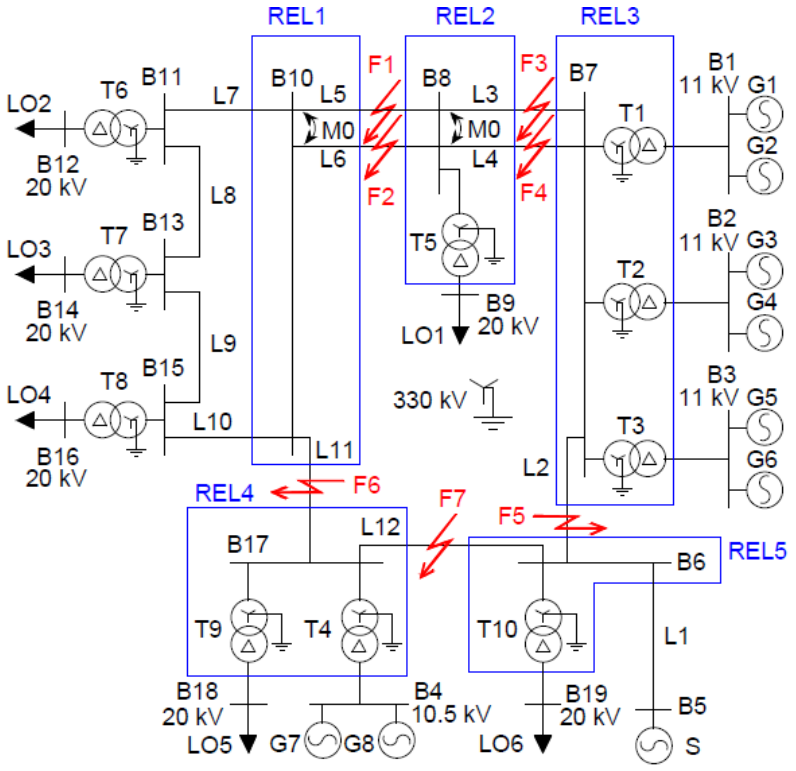

Fig. 2. The case study network.

The scenario groups consider phase-to-earth faults in an OHTL occurring while one or two other lines are out of service (Table 11). The scenario IDs consist of, first, the fault ID and then, the IDs of the lines (according to Fig. 2.) considered offline before the fault. The table also shows the maximum number of measurement phasors available for the developed FL from both ends of the line, if the additional apparent power measurements are not used.

Table 1. Scenarios Modelled in the Case Study

Scenario ID	F1L3	F6L5L6	F5L3L4	F7L2	F7L1
ID of the faulted line	L5	L11	L2	L12	L12
IDs of the disconnected lines	L3	L5 and L6	L3 and L4	L2	L1
Available measurement phasors during the pre-fault state	11	9	9	9	9
Available measurement phasors during the fault state	52	43	43	43	43

For each group of scenarios, 1000 randomised scenarios are generated. In these scenarios, the active power is randomly assigned to load and generation nodes within the limits of 0 %–120 %. The limits applied to the assignment of the reactive power are the same in case of loads but for generators it is −120 %–120 %. When generating random pre-fault and fault state scenarios, restrictions (4)–(12) are applied as well. In cases when the connection with the equivalent power system is lost and the analysed network part has a power supply deficit, the upper limits of the randomly assigned active and reactive power of loads are set so that the remaining load together with nominal network losses should constitute 99 % of the power of the remaining source capacity. After a possible pre-fault state has been obtained, α and R_F are randomly selected, and a steady-state simulation of a fault state is performed. The results of the simulations are then utilised for FL by the developed method as well as by one existing OTMB method and one TTMB method [2] for performance comparisons.

3.2. Results and Discussion

The testing results for the defined scenario groups are assembled in Table 2. The table provides both maximum and mean values of the error moduli of estimates of the equivalent power system sequence impedances (moduli and X/R ratios) for each group of scenarios. The same values are provided for the number of generations N_{GEN} necessary for the convergence of the GA during the second stage of parameter identification, as it would determine the FL computation time after a fault is cleared. For fault distance α and equivalent fault path resistance R_F, the value of two standard deviations is calculated from the moduli of the sub-scenario errors as well. Combined with the mean value, it shows the approximate upper limit of errors to be expected in 95 % of cases. "α REDI1" and "α REDI2" in Table 2 stand for the fault distances calculated by OTMB and TTMB FL algorithms implemented in an existing relay terminal [2].

The results in Table 2 demonstrate the high tolerance of the first estimation stage with only a few cases where the X^1 / R^1 ratio estimation errors approached or exceeded 10 % and show that utilisation of additional measurements would yield little improvement in accuracy for this estimation stage. The observed accuracy can be explained by a low number of decision variables and a sufficient sensitivity of measurement groups to changes in the system PS impedance values. The results for the second estimation

stage show larger errors for estimates of NS and even larger ones for ZS impedances with occasional maximum errors exceeding 20 % and 50 % for $|Z^0_S|$ and X^0 / R^0. However, the mean errors of the moduli of both impedances remain within 5 % for almost all the scenario groups. Furthermore, X / R ratio estimation errors have a noteworthy impact on impedance only when an actual X / R ratio value is small due to the use of the tangent function with limited accuracy. The lower tolerance in the NS and ZS impedance estimates can be attributed to a three times larger number of decision variables compared to the first stage and a higher sensitivity of measurements to α and R_F compared to the system sequence impedances. The fact that NS impedance estimates are more accurate than ZS ones indicates the positive impact of the search space limitation introduced based on the similarities between NS and PS networks. A comparison between the results with and without utilisation of the additional power flow measurements shows the ability of these measurements to increase estimation accuracy for the system sequence impedances by offsetting the relative lack of sensitivity of the measurement sets, especially to the ZS impedance.

The results of estimating fault path resistance R_F demonstrate that this parameter can be estimated with sufficient accuracy (maximum error 1.79 % when the additional power measurements are used and 4.78 % when they are not). It can also be noted that for R_F, the use of the additional power flow measurements may result in a slightly lower estimation tolerance (F1_L3). However, for the more difficult scenario groups F6_L5_L6, F5_L3_L4 and F7_L2, the additional measurements provided an increase of the average accuracy by 34.8 %–43 %.

Table 2. Case Study Results with Errors for Obtained Parameter Estimates

		Scenario ID								
	F1_L3		F6_L5_L6		F5_L3_L4		F7_L2		F7_L1	
Additional measurements from the power system used		No	Yes	No	Yes	No	Yes	No	Yes	No
$\|Z^1_S\|$	maximum error, %	0.42	0.41	0.35	0.46	0.67	0.69	0.71	0.55	–
	mean error, %	0.022	0.021	0.023	0.024	0.022	0.027	0.029	0.032	–
X^1 / R^1	maximum error, %	8.93	7.07	9.63	7.42	6.35	9.08	8.07	11.97	–
	mean error, %	0.390	0.357	0.381	0.374	0.445	0.427	0.517	0.555	–
$\|Z^2_S\|$	maximum error, %	5.26	4.75	11.64	4.85	5.92	4.96	8.54	6.25	–
	mean error, %	0.404	0.347	0.593	0.299	0.589	0.381	0.839	0.519	–
X^2 / R^2	maximum error, %	34.56	35.00	39.73	29.17	41.50	21.83	40.37	25.92	–
	mean error, %	2.293	1.177	2.675	0.299	2.964	1.540	3.319	1.538	–
$\|Z^0_S\|$	maximum error, %	55.66	18.14	51.26	13.54	27.23	10.58	27.49	9.56	–
	mean error, %	7.237	1.506	3.088	1.073	1.739	0.971	1.368	0.957	–

X^0 / R^0	maximum error, %	86.50	42.40	83.67	46.30	68.17	40.57	68.63	39.17	–
	mean error, %	22.643	4.087	12.978	4.498	8.062	4.529	5.854	3.772	–
N_{GEN}	maximum error, %	708	845	958	915	1059	936	1111	1120	796
	mean error, %	427.4	445.0	511.8	489.0	546.9	513.3	575.8	536.4	451.0
R_F	maximum error, %	0.87	0.49	1.51	0.75	4.78	1.19	3.53	1.79	1.24
	mean error, %	0.045	0.052	0.093	0.061	0.169	0.104	0.251	0.143	0.016
	two standard deviations of error, %	0.145	0.161	0.347	0.201	0.709	0.328	0.939	0.474	0.160
α New FL	maximum error, % error, %	0.20	0.41	3.04	2.16	3.50	2.25	4.64	2.93	1.45
	mean error, %	0.030	0.043	0.212	0.159	0.240	0.174	0.469	0.278	0.031
	two standard deviations of error, %	0.078	0.123	0.687	0.472	0.799	0.542	1.517	0.811	0.199
α REDI1	maximum error, %	51.67	56.79	69.74	78.43	96.39	102.12	112.67	121.34	94.08
	mean error, %	7.475	7.784	14.848	15.14	7.182	7.440	9.743	10.290	7.837
	two standard deviations of error, %	17.15	18.04	39.11	39.29	21.36	24.47	28.38	30.10	28.49
α REDI2	maximum error, %	0.20	0.20	0.23	0.23	0.30	0.28	0.19	0.19	0.96
	mean error, %	0.087	0.088	0.103	0.103	0.120	0.121	0.077	0.077	0.431
	two standard deviations of error, %	0.102	0.101	0.115	0.114	0.165	0.147	0.108	0.110	0.491

Overall, the episodically significant errors for estimates of the PS, NS and ZS impedances of the power system and R_F did not critically affect the accuracy of the developed FL. This is shown by α estimation errors remaining within the 4.64 % margin, if additional measurements are not used, and 2.93 %, when they are. The scenario group F1_L3 indicates that for "easier" scenarios, where the measurements used are more sensitive to changes in α, extension of the measurement group with the measurements from the equivalent power system can be slightly counterproductive. However, in "difficult" scenarios, the additional measurements provided a reduction in the maximum error by 0.88 %–1.71 % of faulted line length and narrowed the range of most FL errors as shown by the drop of the error standard deviation value, which was 0.108 %–0.353 %. Data for scenario group F1_L3 in Table 1 and Table 2 indicate that after a sufficient number of available measurements is reached, a further increase

of the measurement set provides little positive impact on the overall accuracy of the developed FL method, matching the observation made in the previous study [13]. Instead, the number of parallel links and the position of the faulted line within the network seem to have a higher importance.

The obtained results (Table 2) also show that the developed FL is significantly more accurate than the existing apparent-reactance-measurement-based FL (REDI1). A comparison with the existing TTMB FL (REDI2) shows that in easier scenarios (F1_L3, F7_L1), the developed FL algorithm is more accurate on average and has a smaller error dispersion as shown by the cumulative distribution functions (CDFs) obtained from scenario results (Fig. 3). However, in the more difficult scenarios, the existing TTMB method outperforms the developed method but only by 0.11 %–0.39 % of faulted line length, if the additional apparent power measurements are disregarded, and by 0.06 %–0.20 % when they are utilised.

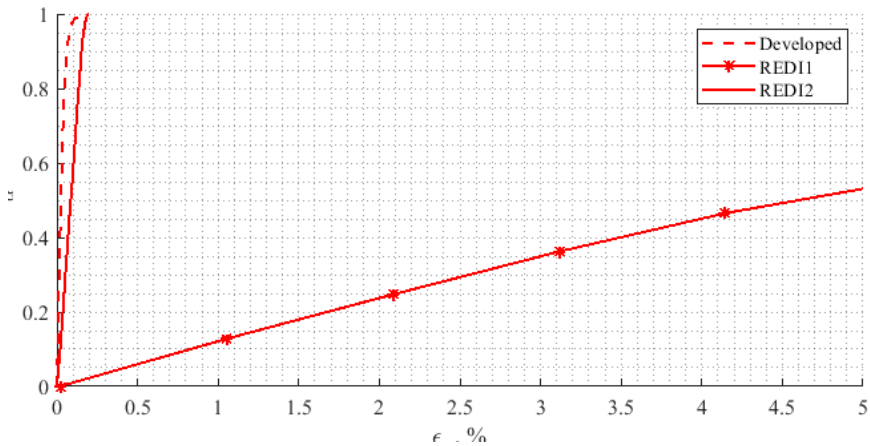

Fig. 3. The CDFs of fault distance estimate error absolute values for scenario F1_L3 without additional apparent power measurements.

4. CONCLUSIONS

The developed method ensures adaptiveness, accuracy, and robustness with a combination of several different approaches. First, models of an analysed network part are made up to date and the PS sequence impedance of an equivalent power system is estimated before fault occurrence. This reduces potential causes for errors, the number of decision variables, and the search space for the optimisation operating after a fault is cleared, thus increasing both the feasibility and accuracy of FL. The updates are performed by utilising information from a SCADA system without strict requirements for data synchronisation; limited data such as the state of CBs and power generation and demand at the main "border" nodes are fetched. Second, the utilised measurement group is extended from just the faulted line to all branches within a particular substation, which has the added benefit of reducing the potential impact of measurement errors. Third, the indirect utilisation of measurement data from the

other end of the line is integrated without a data synchronisation requirement by means of result cross-checks. These allow the FL devices to operate semi-independently and to compensate for the potential lack of sensitivity of a measurement group available at one of the line ends.

The case study results show that the PS impedance of an equivalent power system can be determined with a very good tolerance, allowing the use of its estimate to define the possible interval of NS impedance values with only slightly extended margins. Estimates of the NS impedances are less accurate, but on average, their moduli are determined with a 1 % error margin. The ZS impedance estimates were the least accurate ones due to both a larger search space and a lower sensitivity of measurements to this parameter. When considering X / R ratio estimates, a similar situation is observed, but their inaccuracy often has a limited impact on the sequence impedances due to the use of the tangent function. The use of the additional power flow measurements is most useful for estimation of NS and ZS impedances as they offset the sensitivity of measurement groups towards fault distance and equivalent resistance. The episodically significant errors of estimates of system sequence impedances do not critically affect the accuracy of the developed FL, which remains within the defined 5 % limit. Utilisation of the additional apparent power measurements notably increases the accuracy of the developed FL for relatively difficult scenarios while having little effect for less problematic scenarios. A comparison with two existing FL algorithms demonstrates that developed method outperforms an existing reactance-measurement-based method. Considering simpler scenarios, it also outperforms a TTMB method in all terms but maximum error, however, in more complex scenarios the existing TTMB algorithm has a slightly higher accuracy than the developed FL method.

The future work related to the developed method could entail development and integration of universal models applicable for different fault types occurring in any of OHTLs within an analysed network part. Another research direction could be sensitivity analysis for evaluating and mitigating the impact of measurement errors or changes in the parameters of transmission lines.

ACKNOWLEDGEMENTS

The research has been funded by the Ministry of Economics of the Republic of Latvia, project "Innovative Smart Grid Technologies and their Optimization (INGRIDO)", project No. VPP-EM-INFRA-2018/1-0006.

REFERENCES

1. Takagi, T., Yamakoshi, Y., Yamaura, M., Kondow, R., & Matsushima, T. (1982). Development of a New Type Fault Locator Using the One-Terminal Voltage and Current Data. *IEEE Transactions on Power Apparatus and Systems*, *PAS-101*(8), 2892–2898. DOI: 10.1109/TPAS.1982.317615.
2. Silarajs, M., Utans, A., Leite, L., & Sauhats, A. (2007). Multifunction relay protection device for power transmission lines LIDA. In *Proceedings of the 2nd International Conference on Electrical and Control Technologies*, (pp.120–125). 3–4 May 2007, Kaunas, Lithuania.

3. Blackburn, J.L., & Domin, T.J. (2006). *Protective Relaying Principles and Applications* (3rd ed.). New York: CRC Press.
4. Xu, Z., & Zhang, Z. (2015). What accuracy can we expect from the single-ended fault locator? In *2015 68th Annual Conference for Protective Relay Engineers*, (pp. 690–716). 30 March–2 April, 2015, Texas, USA. DOI: 10.1109/CPRE.2015.7102204.
5. Reddy, C.P., Sarma, D.V.S.S.S., & Varaprasad, O.V.S.R. (2017). A novel fault classifier and locator using one-end current spectrum and minimal synchronized symmetrical components for transmission lines. In *2016 IEEE Annual India Conference*, (pp. 1–6). 16–18 December 2016, Bangalore, Inida. DOI: 10.1109/INDICON.2016.7839128.
6. Davoudi, M.G., Sadeh, J., & Kamyab, K. (2012). Time domain fault location on transmission lines using genetic algorithm. In *2012 11th International Conference on Environment and Electrical Engineering*, (pp. 1087–1092). 18–25 May 2012, Venice, Italy. DOI: 10.1109/EEEIC.2012.6221542.
7. Ahmed, A.S., Attia, M.A., Hamed, N.M., & Abdelaziz, A.Y. (2018). Comparison between genetic algorithm and whale optimization algorithm in fault location estimation in power systems. In *2017 Nineteenth International Middle East Power Systems Conference*, (pp. 631–637). 19–21 December 2017, Cairo, Egypt. DOI: 10.1109/MEPCON.2017.8301247.
8. Pereira, C.E.M., & Zanetta, L.C. (2005). Optimization Algorithm for Fault Location in Transmission Lines Considering Current Transformer Saturation. *IEEE Transactions on Power Delivery*, *20*(2), 603–608. DOI: 10.1109/TPWRD.2004.838521.
9. Jian, Z., HongJun, Z., & JiangFeng, Q. (2012). A two-terminal fault location algorithm using asynchronous sampling based on genetic algorithm. In *2011 International Conference on Advanced Power System Automation and Protection*, (pp. 1513–1516). 16–20 October 2011, Beijing, China. DOI: 10.1109/APAP.2011.6180605.
10. Abedini, M., Hasani, A., Hajbabaie, A. H., & Khaligh, V. (2013). A new traveling wave fault location algorithm in series compensated transmission line. In *2013 21st Iranian Conference on Electrical Engineering*, (pp. 1–6). 14–16 May 2013, Mashhad, Iran. DOI: 10.1109/IranianCEE.2013.6599888.
11. Xun, L., Shungui, L., Ronghui, H., Jingwen, A., Yunzhu, A., Ping, C., & Zhengxiang, X. (2018). Study on accuracy traveling wave fault location method of overhead line–cable hybrid line and its influencing factors. In *2017 Chinese Automation Congress,* (pp. 4593–4597). 20–22 October 2017, Jinan, China. DOI: 10.1109/CAC.2017.8243590.
12. Birjadar, A., & Tajane, S. (2017). Modelling and simulation of transmission line to detect single line to ground fault location. In *2016 IEEE 1st International Conference on Power Electronics, Intelligent Control and Energy Systems*, (pp. 1–4). 4–6 July 2016, Delhi, India. DOI: 10.1109/ICPEICES.2016.7853231.
13. Zālītis, I. (2020). *Application of Estimation of Model Parameters for Protective Automation of Transmission Lines*. PhD Thesis. Riga: RTU.
14. Feng, Z., Jun, L., Li, Z., & Zhihao, Y. (2008). A new fault location method avoiding wave speed and based on traveling waves for EHV transmission line. In *2008 Third International Conference on Electric Utility Deregulation and Restructuring and Power Technologies*, (pp. 1753–1757). 6–9 April 2008, Nanjing, China. DOI: 10.1109/DRPT.2008.4523690.
15. Altaie, A.S., & Asumandu, J. (2017). Fault location using a new control technique, multiple classifier, and artificial neural network. In *2017 IEEE Texas Power and Energy Conference*, (pp. 1–6). 9–10 February 2017, Texas, USA. DOI: 10.1109/TPEC.2017.7868267.
16. Ayyagari, S.B. (2011). *Artificial Neural Network Based Fault Location for Transmission Lines*. M.S. Thesis. Lexington: UKnowledge. URL: https://uknowledge.uky.edu/gradschool_theses/657.

17. Kezunovic, M., & Knezev, M. (2008). Selection of optimal fault location algorithm. In *2008 IEEE Power and Energy Society General Meeting – Conversion and Delivery of Electrical Energy in the 21st Century*, (pp. 1–5). 20–24 July 2008, Pittsburgh, Pennsylvania. DOI: 10.1109/PES.2008.4596775.
18. Keshri, J.P., & Tiwari, H. (2017). Parameter-less fault locator using synchronized/un-synchronized data for overhead transmission line. In *2017 International Conference on Computer, Communications and Electronics*, (pp. 260–264). 1–2 July 2017, Jaipur, India. DOI: 10.1109/COMPTELIX.2017.8003975.
19. Farshad, M., & Sadeh, J. (2012). Transmission Lines Based on k-Nearest Neighbour Algorithm Using One-End Voltage. *IEEE Transactions on Power Delivery*, *27*(4), 2360–2367. DOI: 10.1109/TPWRD.2012.2211898.
20. Bockarjova, M., Dolgicers, A., & Sauhats, A. (2008). Enhancing fault location performance on power transmission lines. In 2007 IEEE Lausanne Power Tech, (pp. 1123–1128). 1–5 July 2007, Lausanne, Switzerland. DOI: 10.1109/PCT.2007.4538473.
21. Voldek, A.I., & Popov, V.V. (2007). *Electrical Machines*. *Alternating Current Machines*. St. Petersburg: Peter Press. ISBN: 978-5-469-01381-5 (in Russian).
22. Chen, C.S., Liu, C.W., & Jiang, J.A. (2006). Application of Combined Adaptive Fourier Filtering Technique and Fault Detector to Fast Distance Protection. *IEEE Transactions on Power Delivery*, *21*(2), 619–626. DOI: 10.1109/TPWRD.2005.858808.
23. Geramian, S.S., Abyane, H.A., & Mazlumi, K. (2008). Determination of optimal PMU placement for fault location using genetic algorithm. In *2008 13th International Conference on Harmonics and Quality of Power*, (pp. 1–5). 28 September–1 October 2008. DOI: 10.1109/ICHQP.2008.4668810.
24. He, L., Jia, K., & Fan, Z. (2010). The immune genetic algorithm in fault diagnosis of modern power system. In *2010 2nd International Conference on Education Technology and Computer,* (pp. 26–29). 22–24 June 2010, Shanghai, China. DOI: 10.1109/ICETC.2010.5529742.
25. Cruz, H.O., & Leão, F.B. (2018). Optimal placement of fault indicators using adaptive genetic algorithm. In *2017 IEEE Power & Energy Society General Meeting*, (pp. 1–5). 16–20 July 2017, Chicago, Illinois, USA. DOI: 10.1109/PESGM.2017.8273897.